Nanoscale

Accepted Manuscript

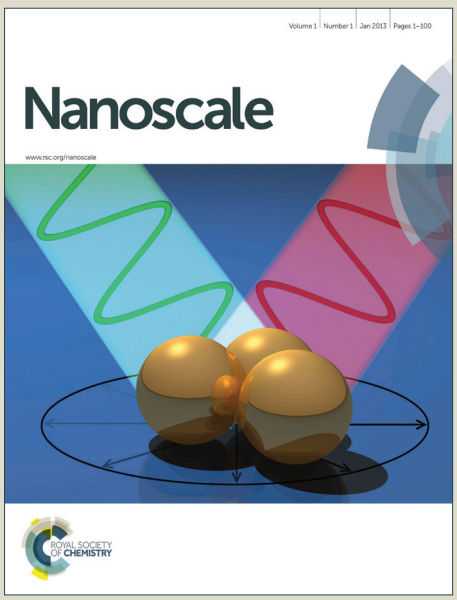

ROYAL SOCIETY OF CHEMISTRY

www.rsc.org/nanoscale

Cite this: DOI: 10.1039/c0xx00000x

www.rsc.org/xxxxxx

Paper

Nickel Cobalt Oxide/carbon Nanotubes Hybrid as a High-performance Electrocatalyst for Metal/air Battery

Hui Zhang[a], Hang Qiao[a], Haiyan Wang[a*], Nan Zhou[b], Jiajie Chen[a], Yougen Tang[a*], Jingsha Li[a], Chenghuan Huang[c]

Received (in XXX, XXX) Xth XXXXXXXXX 20XX, Accepted Xth XXXXXXXXX 20XX
DOI: 10.1039/b000000x

High-performance catalyst for oxygen reduction reaction (ORR) with low cost remains a big challenge. Herein, nanostructured $NiCo_2O_4$/CNTs hybrid was proposed as a high-performance catalyst for metal/air battery for the first time. The well-formed $NiCo_2O_4$/CNTs hybrid was studied by the steady-state linear polarization curves and the galvanostatic discharge curves in comparison with CNTs-free $NiCo_2O_4$ and the commercial carbon-supported Pt. Due to the synergistic effect, the $NiCo_2O_4$/CNTs hybrid exhibited significant improvement of catalytic performance in comparison with the $NiCo_2O_4$ or CNTs alone, which even outperformed the Pt/C hybrid in ORR process. Also, the benefits of Ni incorporation was demonstrated by the improved catalytic performance of $NiCo_2O_4$/CNTs compared to Co_3O_4/CNTs, which should be ascribed to the improved electrical conductivity and new highly efficient active sites created by the Ni cation incorporation into the spinel structure. The $NiCo_2O_4$/CNTs hybrid could be used as a promising catalyst for high power metal/air battery.

1 Introduction

The ever-growing energy demand has greatly stimulated recent researches on exploiting high performance electrode materials for energy-storage devices.[1-3] Metal/air battery,[4, 5]especially aluminum/air battery,[6, 7] has been considered as one of the most promising energy-storage devices because of their high energy density, low operating temperature and low cost.[6] The actual energy density of aluminium/air (oxygen) battery can reach 600-800 Wh kg^{-1}, which is far higher than Li ion battery.[8] Its structure and materials can be determined according to the demand of users, which has excellent adaptability. In addition, aluminium is the one of the most abundant metal and the third most abundant element in the earth's crust. Therefore, aluminum/air battery turns out to be the more promising green power system for electric vehicles.

The air electrode is crucial to the electrochemical performance of aluminium/air batteries.[9, 10] There are various factors that affect the performance of the air electrodes in metal/air batteries. High-performance catalysts for the oxygen reduction reaction (ORR) are the most important components of air electrode.[11] Up to now, platinum-based materials are known to be the most active catalysts for ORR in both acidic and alkaline conditions.[12-16] But the high cost hinders their large-scale applications. Therefore, it is of great importance to reduce Pt content in the catalysts or explore new high-performance ORR catalysts comparable to Pt/C with much lower cost.

Mixed valence oxides of transition metals with a spinel structure are an important class of metal oxides that exhibit fine ORR catalytic activity in alkaline conditions.[17] Due to their prominent advantages of low price, easy preparation, environmental friendliness, high activity and high stability, spinel cobalt-based oxides have been researched extensively.[18-22] In particular, ternary nickel cobalt oxides ($NiCo_2O_4$), in which one Co atom in Co_3O_4 is substituted with Ni have recently been investigated as a high-performance electrocatalysts for ORR because of its better electrical conductivity and higher electrochemical activity compared with NiO and Co_3O_4.[18, 23] Several different types of $NiCo_2O_4$ nanostructures have been synthesized and their electrochemical performance has been investigated. Yang and his co-workers fabricated $NiCo_2O_4$ spinel nanowire arrays as a bifunctional catalyst for oxygen reduction and evolution reaction.[24] In addition, urchin-like $NiCo_2O_4$ spheres have also been obtained through hydrothermal method, exhibiting excellent ORR activity.[22] However, spinel oxides still exhibit a much lower activity compared to commercial carbon-supported Pt. To further enhance the electrochemical performance, one of the key strategies is to develop a composite material to maximize the electroactive surface and improve the electrical conductivity of the catalysts simultaneously.[25] CNTs show high electrical conductivity, large surface area, high mechanical strength, and structural flexibility, making them the ideal substrates for supporting such nanocrystal catalysts.[26] Despite that some researches have reported $NiCo_2O_4$/CNTs as a high-performance electrode for supercapacitor,[25, 27] however, to the best of our knowledge, there is no paper involving the electrochemical studying as electrocatalyst for the ORR process.

In this work, we deposited $NiCo_2O_4$ nanoparticles on the surface of CNTs by a facile solution method combined with a simple thermal treatment as an active electrocatalyst for ORR. Note that the synthesis method for $NiCo_2O_4$/CNTs was very simple and low cost. The electrochemical activities of the hybrid towards ORR were evaluated in a home-made aluminum/air battery model under the alkaline condition. The $NiCo_2O_4$/CNTs electrode delivered superior electrochemical catalytic performance under high current density in comparison with commercial carbon-supported Pt (5wt% Pt. J&K). We also demonstrated the benefits of incorporating Ni cation into the spinel lattice by comparing the electrocatalytic activity of $NiCo_2O_4$/CNTs with Co_3O_4/CNTs.

2 Experiment

2.1 Catalyst preparation

The oxidized CNTs were functionalised by a well-known acid oxidation method to introduce oxygenous groups for increasing the surface activity of CNTs. CNTs with 30-70 nm diameter and 1-2 μm length (Chengdu Organic Chemicals Co. Ltd.) were first purified by calcinations at 500 °C for 0.5 h. Then, the purified CNTs (1 g) and 60 ml of nitric acid（65%-68%）were put into a 100 ml round-bottom flask, and the mixture was refluxed at 110 °C for 10 h. The product was collected through centrifugation and washed with distilled water and ethanol for several times. $NiCo_2O_4$/CNTs was controllably synthesized through a facile hydrothermal approach combined with appropriate thermal treatment. Typically, a certain quantity of functionalised CNTs was dispersed into 20 ml of ethanol and sonicated for 50 min to reach good dispersion. Then, 1 mmol of $Ni(NO_3)_2{\cdot}6H_2O$, 2 mmol of $Co(NO_3)_2{\cdot}6H_2O$ and 4.5 mmol of hexamethylenetetramine were dissolved into 40 ml of distilled water to form a transparent pink solution. The above two solutions are then mixed and heated to 90 °C in an oil bath for 4 h. After the solution was cooled down to room temperature naturally, the product was collected through centrifugation and washed with distilled water and ethanol for several times. The products were then dried at 60 °C in a vacuum oven for 24 h, followed annealing process at 350 °C for 2 h in a muffle furnace with a slow heating rate of 5 °C min^{-1} to get $NiCo_2O_4$/CNTs hybrid nanostructures.

For comparison, CNTs-free $NiCo_2O_4$ was synthesized by the same method as $NiCo_2O_4$/CNTs hybrid but without adding CNTs in the first step. Co_3O_4/CNTs hybrid was prepared through the same steps as $NiCo_2O_4$/CNTs hybrid without adding any Ni salt in the first step. Free Co_3O_4 was synthesized through the same steps as $NiCo_2O_4$ without adding any Ni salt in the first step. It should be noted that the control experiment about the contents of CNTs was performed to optimize the catalytic activity of the hybrid. The results suggested that the hybrid with ca. 12 wt % CNTs displayed the best ORR performance (Fig. S1-S3, ESI). So the $NiCo_2O_4$/CNTs hybrid with 12 wt % CNTs was further characterized.

2.2 Characterizations

The as-prepared products were characterized by the Dandong X-ray diffractometer (DX-2700) utilizing a Cu-Kα1 source with a step of 0.02°. The surface morphology of the products was observed by scanning electron microscopy (Quanta FEG 250). Transmission electron microscopy (TEM) and high resolution TEM (HRTEM) images were recorded with a F 20 microscope. X-ray energy dispersive spectroscopy (EDS) and X-ray photoelectron spectroscopy (XPS, K-Alpha1063) were applied to research the chemical compositions of the samples. Thermogravimetric analysis (TGA) and differential scanning calorimetry (DSC) were carried out with a STA 449 C Jupiter thermogravimetric analyzer (NETZSCH) in the temperature range from 40 to 700 °C in air at a heating rate of 10 °C min-1. The Brunauer-Emmett-Teller (BET) surface area of the samples was detected by nitrogen adsorption/desorption at -196°C using a Builder SSA-4200 apparatus. Before the measurement, the samples were degassed at 150 °C for 3 h under vacuum. The electrical conductivities of the materials were measured at room temperature by a four-point probe conductivity measurement (SDY-40, Guangdong, China), in which the powder was pressed in a stainless steel die for 0.5 h with P =20 MPa in a compressor.

2.3 Fabrication of air electrode and electrochemical characterizations

To study the electrocatalytic activities of the samples, catalysts were loaded onto air electrodes. The air electrode is a three-layer structure, which contains the gas diffusion layer, current collector, the catalytic layer. The nickel foam was used as the current collector in air electrode for its good conductivity and high intensity. The catalytic layer was fabricated as follows: catalysts, active carbon and acetylene black, polytetrafluoroethylene (PTFE) were mixed well in a weight ratio of 3:3:1:3, then the paste was rolled until the thickness of this layer was about 0.2 mm. Finally, the film was pressed onto nickel foam (2 cm × 5 cm) at 15 MPa and then dried at 60 °C for 12 h. For comparison, a commercially available 5 wt% Pt/C (J&K) catalyst was used. The air electrode using the Pt/C as the catalyst was obtained by the same process.

The linear polarization curves and galvanostatic discharge curves were carried out using a CHI660D electrochemical workstation system (Shanghai Chenhua, China) in a three-electrode cell by using the air electrode as the working electrode, Hg/HgO electrode as the reference electrode and a platinum foil as the counter electrode. The electrolyte was a 6.0 M KOH aqueous solution. On the other hand, for full cell tests, the electrolyte was composed of 6 M KOH and 0.01 M Na_2SnO_3, 0.0005 M $In(OH)_3$, 0.0075 M ZnO as corrosion inhibitors. The apparatus used for electrochemical measurements was the home-made model. The more details are shown in literature.[8]

3 Results and discussion

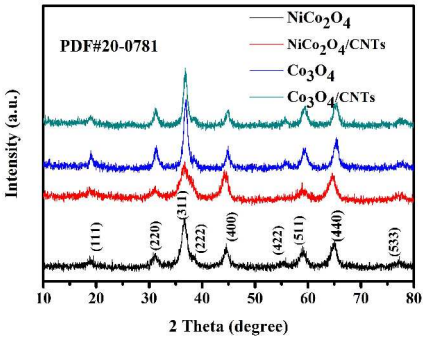

Fig. 1 XRD patterns of the as-prepared pure $NiCo_2O_4$ (back), $NiCo_2O_4$/CNTs hybrid (red), pure Co_3O_4 (blue) and Co_3O_4/CNTs hybrid (green).

3.1 Structure and morphology of catalysts

Fig. 1 shows typical XRD patterns of the as-prepared materials. Apparently, nine characteristic diffraction peaks, including their peak positions for the four samples can be well indexed to crystal planes of the cubic spinel phase.[28] In the case of $NiCo_2O_4$/CNTs, the XRD pattern lines are in good agreement with the standard card (JCPDS No. 20-0781). No other impurity peak could be seen, indicating the sample is of high purity. It should be noted that the XRD pattern lines of $NiCo_2O_4$/CNTs are relatively broader compared to those of Co_3O_4/CNTs, which is indicative of formed smaller crystallites due to the addition of Ni atoms into the spinels of Co_3O_4.[29] According to the Scherrer's equation, the crystal size of $NiCo_2O_4$/CNTs particle is determined to be 9.02 nm, much less than that (13.41 nm) of Co_3O_4/CNTs. The cubic lattice parameter *a* of the as-synthesized $NiCo_2O_4$ is calculated to be 8.111 Å, slightly larger than that of 8.081 Å for the cubic Co_3O_4, which is consistent with the literature because the incorporation of Ni into the Co_3O_4 spinel could expand the elementary spinel lattice.[30, 31] This can clearly ascertain the formation of the $NiCo_2O_4$ phase after annealing at 350 °C for 2 h in a muffle furnace, which indicates that the temperature of 350°C is high enough to convert its precursors into $NiCo_2O_4$ by an oxidation reaction in air as follows:

$$2Co(OH)_2 + Ni(OH)_2 + 1/2O_2 \rightarrow NiCo_2O_4 + 3H_2O \quad (1)$$

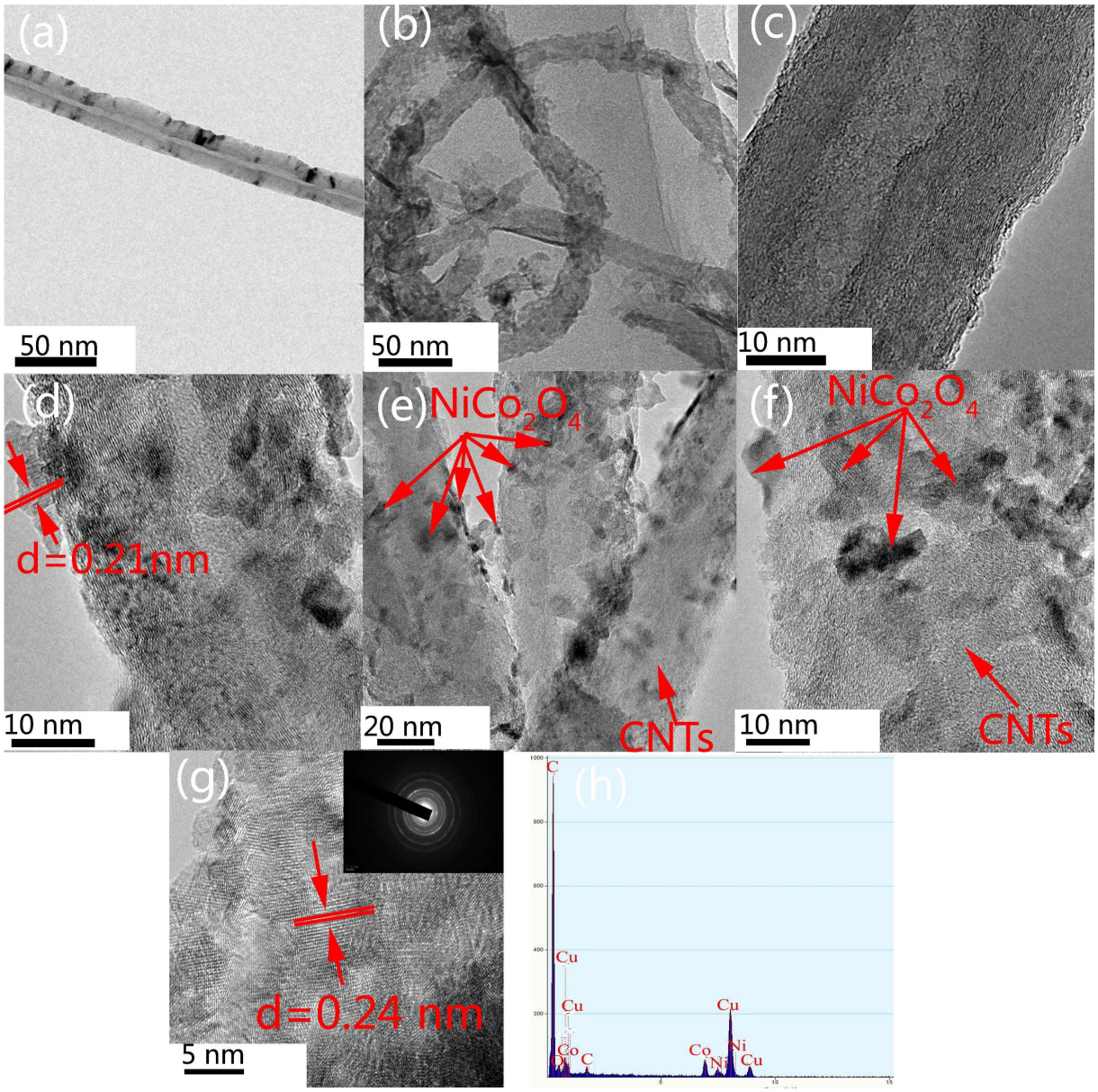

Fig. 2 TEM images of bare CNTs (a), $NiCo_2O_4$/CNTs (b) and a high-magnification TEM image of bare CNTs (c), $NiCo_2O_4$/CNTs (d); TEM images of $NiCo_2O_4$ uniformly distributed on CNTs (e-f); HRTEM image of $NiCo_2O_4$ nanoparticles together with the SAED pattern inset (g); An EDS spectrum of $NiCo_2O_4$/CNTs hybrid (h)

The morphology and structure of the as-synthesized $NiCo_2O_4$/CNTs were characterized by transmission electron microscopy (TEM) and high-resolution TEM (HRTEM). The bare CNTs present a clean surface with no heterophase nanoparticles (Fig. 2(a)). However, as shown in Fig. 2(b), the composite surface is dotted homogeneously with $NiCo_2O_4$ nanoparticles. Comparing Fig. 2c with Fig. 2d, there is only one kind of uniform strip in Fig. 2(c), related to the lattice fringes of CNTs. But in Fig. 2(d), there appear clear lattice fringes with a d-spacing of 0.21 nm which can be well indexed to the (400) plane of cubic $NiCo_2O_4$. It can be clearly observed (Fig. 2(e) and Fig. 2(f)) that the size of $NiCo_2O_4$ nanoparticles is less than 10 nm and are well formed on the surface of CNTs. The high crystallinity of the nanoparticles has been also confirmed by SAED, which shows the polycrystalline nature of the $NiCo_2O_4$ nanoparticles (Fig. 2(g)). Moreover, the presence of $NiCo_2O_4$ was further confirmed by EDS result, as shown in Fig. 2(h). The Ni and Co peaks ensure the presence of the ternary oxide. The C peak is from the CNTs, and the Cu peak is from the TEM grid.

To obtain more detailed elemental composition and the oxidation state of $NiCo_2O_4$/CNTs hybrid, XPS measurement was performed and the corresponding results are shown in Fig. 3(a)-(d). A full survey of $NiCo_2O_4$/CNTs in Fig. 3(a) reveals the existence of Ni 2p, Co2p, O 1s, and C1s. By using a Gaussian fitting method, the Co 2p emission spectrum (Fig. 3(b)) was well fitted with two spin-orbit doublets, including the Co^{2+} ions at binding energies of 779.5 eV and 794.6 eV, and Co^{3+} at 780.8 eV and 795.9 eV.[32-34] The Ni 2p emission spectrum (Fig. 3(c)) was

also fitted with two spin-orbit doublets. The fitting peaks at binding energies of 853.7 eV and 872.9 eV are ascribed to Ni^{2+}, while the peaks at 855.2 and 874.5 eV are due to Ni^{3+}.[32-34] The O 1s emission spectrum can be divided into two main peaks (Fig. 3(d)) which have been denoted as O 1, O 2. The fitting peak of O 1 at 529.6 eV is typical of metal oxygen bonds.[33, 35] The well-resolved O 2 component corresponds to a high number of defect sites with low oxygen coordination in the material with small particle size.[36] Obviously, the XPS data suggest that the surface of $NiCo_2O_4$/CNTs hybrid has a composition containing Co^{2+}, Co^{3+}, Ni^{2+}, and Ni^{3+}. Thus, the formula of $NiCo_2O_4$ can be generally written as follow: $Co^{2+}_{1-x}Co^{3+}_x[Co^{3+}Ni^{2+}_xNi^{3+}_{1-x}]O_4$ ($0 < x < 1$) (the cations within the square bracket are in octahedral sites and the outside ones occupy the tetrahedral sites).[37, 38] In addition, the XPS shows that the atomic ratio of Co to Ni is close to 2:1, in a good agreement with the designed ratio of $NiCo_2O_4$.

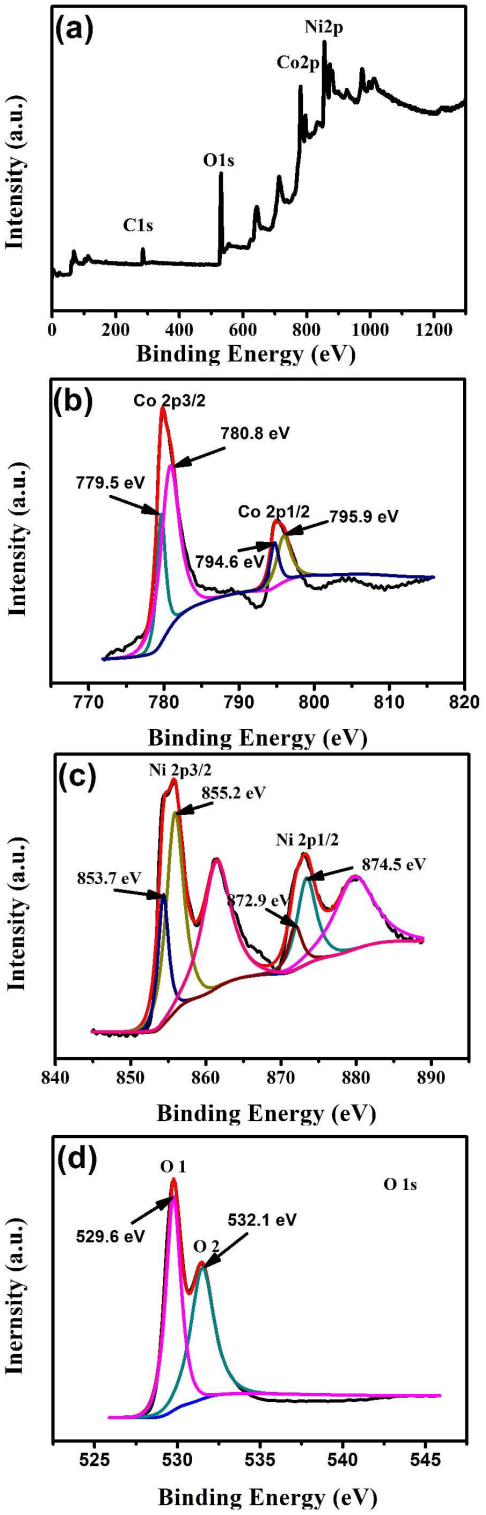

Fig. 3 XPS spectra of survey spectrum (a), Co 2p (b), Ni 2p (c) and O 1s (d) for $NiCo_2O_4$/CNTs hybrid.

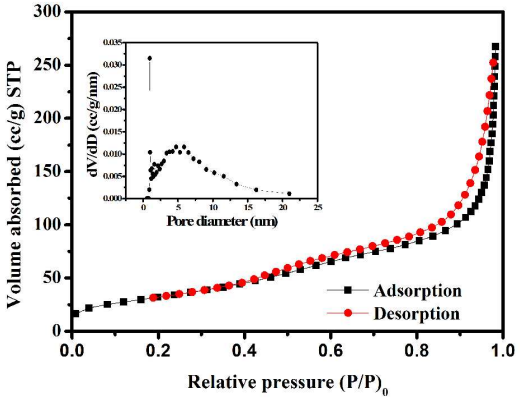

Fig. 4 N_2 adsorption-desorption isotherm and pore size distribution (inset) of the $NiCo_2O_4$/CNTs hybrid

N_2 adsorption-desorption measurement was carried out. According to the International Union of Pure and Applied Chemistry (IUPAC) classification, the isotherm of $NiCo_2O_4$/CNTs can be ascribed to a type of IV isotherm with the H_3 type hysteresis loop in the relative pressure range of 0.5-0.95 (Fig. 4), suggesting the presence of mesoporous structure.[29] A high BET surface area of 121.6 m^2 g^{-1} is demonstrated, which should be attributed to the high surface of CNTs and /or the presence of the ultrafine $NiCo_2O_4$ nanoparticles deposited on CNTs.[39] The high specific surface area may enhance the exposure of active sites available for ORR on the three-phase interface. The porous feature is further confirmed by the pore size distribution result (Fig. 4, inset), indicating two predominant peaks in the micro-sale of 1 nm and meso-sale of 2 to 10 nm with an average pore diameter of 5 nm (Fig.2(e)). The micropores may come from the CNTs and the formation of the mesopores could be attributed to the gas release during the decomposition of the Ni-Co precursor synthesized using the hexamethylenetetramine as the capping reagent. It is worthwhile noting that the porous structure is very important to offer more active sites for an easy access of the adsorption of gas, thereby enhancing the utilization of active sites during the ORR.[40]

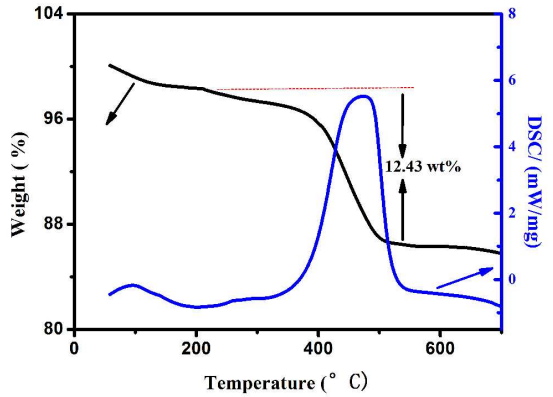

Fig. 5 DSC/TG curves of as-prepared $NiCo_2O_4$/CNTs hybrid

Fig. 5 shows the DSC/TG result of $NiCo_2O_4$/CNTs hybrid. As can be seen, there is a weight loss of about 2.8 wt. % from 50 °C to 100 °C with an endothermic peak at about 99.5 °C in DSC curve, corresponding to the evaporation of physical adsorbed water.[41] The weight loss about 12.43 wt. % in the temperature range between 200 and 540 °C in TG curve should be related to the reduction of CNTs. There is a big exothermic peak at about 475 °C in DSC curve which corresponds to the reaction between CNTs and O_2. When the temperature is over 540 °C, there is no weight loss, indicating that the content of the carbon nanotubes in the composite is about 12.43%. Note that there is only a slight weight loss before 350 °C, confirming that almost CNTs could be retained during the annealing process at 350 °C for 2 h in air.

3.2 Electrochemical performance

The electrochemical properties of $NiCo_2O_4$/CNTs hybrid were well conducted by using the three-electrode half-cell testing. The catalysis of ORR using the $NiCo_2O_4$/CNTs hybrid as the electrocatalyst was studied by the steady-state linear polarization curves (LSV) in 6.0 M KOH aqueous solution with a scan rate of 2 mV s^{-1} and compared with other catalysts at ambient temperature. The tested voltage ranges from 0.2 to -0.6 V. Control experiments for commercial Pt/C hybrid were also carried out under the same conditions. As can be seen from Fig. 6, the black curve, relating to $NiCo_2O_4$/CNTs hybrid was the steepest one in all, indicating the best electrocatalytic activity, which exceeds that of Pt/C hybrid in 6.0 M KOH. The high-performance electrocatalytic activity of $NiCo_2O_4$/CNTs should be attributed to the increased number of active sites for ORR surface reaction. In terms of the current density, when the potential voltage is -0.6 V, the $NiCo_2O_4$/CNTs hybrid exhibits a much higher value of 525 mA cm^{-2} than that of Co_3O_4/CNTs (395 mA cm^{-2}). The superior electrochemical activity of the hybrid towards ORR is ascribed to the incorporation of Ni cation into the spinel structure as observed by a much enhanced ORR current density compared to that of Co_3O_4/CNTs with the same structure. In the ORR process, Ni cation not only effectively activates Co cation, but also enables the gas molecules to easily permeate and adsorb onto the pore network of the nanoparticles through electrostatic interaction, leading to high efficient ORR reaction.[42] This result also suggests that the spinel oxide nanocrystals on multi-wall carbon nanotubes were the active sites in the hybrid materials.[43]

It should be noted that CNTs-free $NiCo_2O_4$ nanoparticles exhibit certain ORR catalytic activity than that of bare Co_3O_4. CNTs without any metal oxides show very poor ORR catalytic activity. It is clearly observed that both $NiCo_2O_4$/CNTs and Co_3O_4/CNTs hybrid exhibit a much higher current density than their bare materials under the same potential voltage, suggesting the synergistic effect between metal oxides and CNTs.[44-46]. In addition, the oxygenated groups on the surface of the CNTs may facilitate oxygen reduction, which was reported by Kinoshita.[47]. The linear polarization curves of the hybrid shows a significantly higher current density, which is attributed to the increased number of active sites for ORR. In the hybrid, the CNTs can serve as both a supporter for catalysts dispersion to prevent agglomeration of nanoparticles, and provide efficient conduction network for shuttling electrons involved in redox reaction, thereby increasing the number of active sites.[43] It is noted that the catalytic activity of $NiCo_2O_4$/CNTs hybrid depends critically on the amount of CNTs. Too much CNTs may cause the free CNTs, thus deteriorate the ORR activity. The control experiment was performed to optimize the catalytic activity of the hybrid by systematically changing the contents of CNTs. The results suggested that the hybrid with ca. 12 wt % CNTs displayed the best ORR performance (Fig. S1-S3, ESI).

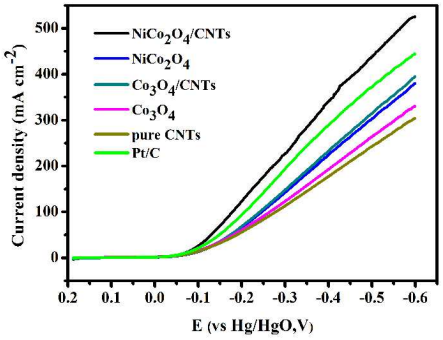

Fig. 6 The linear polarization curves of air electrodes with different catalysts in 6 M KOH solution at 25 °C

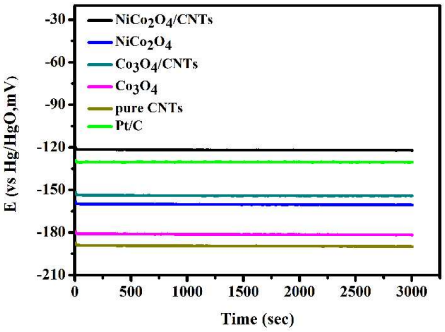

Fig. 7 Galvanostatic discharge curves of air electrodes with different catalysts in 6 M KOH solution at a discharge current density of 50 mA cm^{-2}

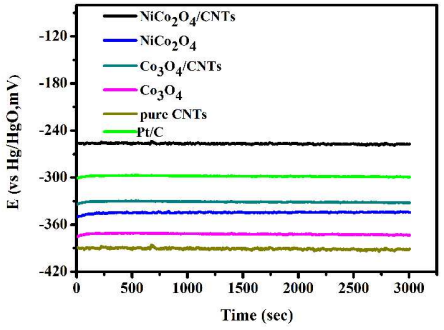

Fig. 8 Galvanostatic discharge curves of air electrodes with different catalysts in 6 M KOH solution at a discharge current density of 200 mA cm^{-2}

The superior ORR activity of the $NiCo_2O_4$/CNTs hybrid can be further confirmed by the galvanostatic discharge curves. From Fig. 7, when the discharge current density is 50 mA cm^{-2}, the stable potential of air electrode with $NiCo_2O_4$/CNTs hybrid is -0.12 V, which is the high-class to those of pure $NiCo_2O_4$, Co_3O_4 and Co_3O_4/CNTs hybrid, and a little higher than the commercial Pt/C. In order to further evaluate the catalytic properties of the $NiCo_2O_4$/CNTs, the catalytic properties at a higher current density of 200 mA cm^{-2} are well compared, as shown in Fig. 8. As observed, the stable potential of air electrode with $NiCo_2O_4$/CNTs hybrid is -260 mV, which is 40 mV higher than that of Pt/C. The enhancement in the stable potential of the hybrid may be attributed to the increase of the electrical conductivity benefiting from the CNTs, which is highly desirable for fast charge transfer during ORR. The electrical conductivities of the materials are measured at room temperature by a four-point probe conductivity measurement. The electrical conductivities of Co_3O_4, Co_3O_4/CNTs, $NiCo_2O_4$ and $NiCo_2O_4$/CNTs are 0.14 S cm^{-1}, 0.45 S cm^{-1}, 7.61 S cm^{-1} and 15.51 S cm^{-1}, respectively. It is clearly observed that both $NiCo_2O_4$/CNTs and Co_3O_4/CNTs hybrid exhibit a much higher electrical conductivity than their bare materials. And the incorporation of Ni atom into the Co_3O_4 contributes to the improvement of electrical conductivity. More importantly, the improved dispersion of metal oxides over the surfaces of the CNTs favors oxygen adsorption on the surface of the hybrid, facilitating electron transfer through the films and decreasing the ORR overpotential.[47] In addition, a significant increase in the stable potential of the $NiCo_2O_4$/CNTs hybrid is indicative of increased accessibility of O_2 onto the active sites for enhancing ORR activity, which could be attributed to the smaller crystallite size of the $NiCo_2O_4$/CNTs hybrid shown from the broad peaks of the XRD pattern.[29] Apparently, the $NiCo_2O_4$/CNTs hybrid demonstrates much better catalytic performance on ORR process under high current density and it could be used as a promising catalyst for high power metal/air battery.

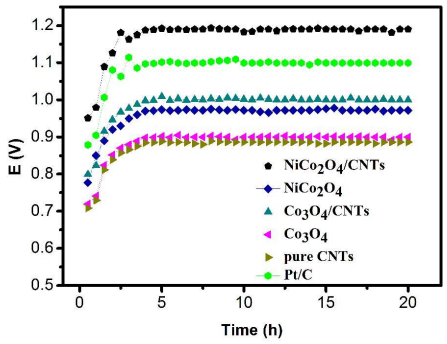

Fig. 9 Constant current discharge tests for the aluminium/air batteries at a discharge current density of 200 mA cm^{-2}

It is of practical significance to characterize the electrocatalytic activity of $NiCo_2O_4$/CNTs on ORR process in aluminum/air batteries. We fabricated a home-made aluminum/air battery for constant current discharge tests. The constant current discharge curve of aluminum/air batteries with $NiCo_2O_4$/CNTs as the cathode catalyst is compared with the commercial Pt/C in Fig. 9. The discharge time was 20 hours and the data were recorded every 0.5 h. After about two hours, the passive film on the surface of the aluminum alloy anode was dissolved in the alkaline medium and the temperature of the electrolyte increased slowly, i.e., the so-called activation process. The working voltage plateau of the cells with $NiCo_2O_4$/CNTs as electrocatalyst is about 1.2 V, which is 0.1 V higher than that of Pt/C. This result is consistent with the results of the steady-state linear polarization curves and the galvanostatic discharge curves, as shown in Fig. 6-8. The better performance of the aluminum/air battery with $NiCo_2O_4$/CNTs as the cathode catalyst indicates that the $NiCo_2O_4$/CNTs hybrid is a promising candidate as the cathode ORR catalyst in alkaline solution.

4 Conclusion

In summary, nanostructured $NiCo_2O_4$/CNTs hybrid was first proposed as a high activity ORR electrocatalyst for air electrode in aluminum/air battery. The catalytic performance on ORR activities was investigated by the steady-state linear polarization curves and the galvanostatic discharge curves measurements. Although $NiCo_2O_4$ or CNTs alone has low catalytic activity, their hybrid exhibits superior ORR activity probably arising from the synergistic effect between metal oxides and CNTs, which even outperformed the commercial carbon-supported Pt. Furthermore, the incorporation of Ni cation into the spinel lattice is observed to significantly improve ORR performance of $NiCo_2O_4$/CNTs. This is ascribed to the increased electrical conductivity and new highly efficient active sites with lower activation energy due to the incorporation of Ni cation into the spinel structure. The high-performance $NiCo_2O_4$/CNTs hybrid could be used as a suitable catalyst for high power metal/air battery.

Acknowledgments

The authors greatly appreciate the financial support from the National Nature Science Foundation of China (No.21271187 and No.21301193), Hunan Provincial Natural Science Foundation of China (No.14JJ3022), Fundamental Research Funds for the Central Universities of Central South University and the Open-End Fund for Valuable and Precision Instruments of Central South University (CSUZC201418).

Notes and References

[a] *College of Chemistry and Chemical Engineering, Central South University, Changsha, 410083, P.R. China.* Tel.: +86-731-88830 886; Fax: +86-731-88879616. *E-mail:* wanghy419@126.com; ygtang@csu.edu.cn.
[b] *College of Science, Hunan Agricultural University, Changsha, 410128, P.R.China.*
[c] *Hunan Changyuan Lico Co., Ltd., Changsha, 410205, P.R. China.*

† Electronic Supplementary Information (ESI) available: [the linear polarization curves and galvanostatic discharge curves of $NiCo_2O_4$/CNTs with different contents of CNTs]. See DOI: 10.1039/b000000x/

1 G. Q. Zhang and X. W. Lou, *Advanced Materials*, 2013, **25**, 976-979.
2 X. W. Lou, L. A. Archer and Z. C. Yang, *Advanced Materials*, 2008, **20**, 3987-4019.
3 C. Liu, F. Li, L. P. Ma and H. M. Cheng, *Advanced Materials*, 2010, **22**, E28-E62.
4 F. Y. Cheng and J. Chen, *Chemical Society Reviews*, 2012, **41**, 2172-2192.
5 Z. L. Wang, D. Xu, J. J. Xu and X. B. Zhang, *Chemical Society Reviews*, 2014, DOI: 10.1039/c3cs60248f.
6 M. Nestoridi, D. Pletcher, R. J. K. Wood, S. Wang, R. L. Jones, K. R. Stokes and I. Wilcock, *Journal of Power Sources*, 2008, **178**, 445-455.

7 S. H. Yang and H. Knickle, *Journal of Power Sources*, 2003, **124**, 572-585.
8 Y. G. Tang, H. Qiao, H. Y. Wang, P. P. Tao, *Journal of Materials Chemistry A*, 2013, **10**, 1-6.
9 F. Bidault, D. J. L. Brett, P. H. Middleton and N. P. Brandon, *Journal of Power Sources*, 2009, **187**, 39-48.
10 Ø. Hasvold, K. H. Øistein, Ole Mollestad, S. Forseth, N. Størkersen, *Journal of Power Sources*, 1999, **80**, 254-260.
11 Y. Y. Liang, D. Q. Wu, X. L. Feng and K. Müllen, *Advanced Materials*, 2009, **21**, 1679-1683.
12 R. Srivastava, P. Mani, N. Hahn and P. Strasser, *Angewandte Chemie International Edition*, 2007, **46**, 8988-8991.
13 A. Morozan, B. Jousselme and S. Palacin, *Energy & Environmental Science*, 2011, **4**, 1238-1254.
14 H. A. Gasteiger, S. S. Kocha, B. Sompalli and F. T. Wagner, *Applied Catalysis B: Environmental*, 2005, **56**, 9-35.
15 H. Wang, R. F. Wang, H. Li, Q. F. Wang, J. Kang and Z. Q. Lei, *InternationalJournal of Hydrogen Energy*, 2011, **36**, 839-848.
16 W. Wang, R. F. Wang, S. Ji, H. Q. Feng, H. Wang and Z. Q. Lei, *Journal of Power Sources*, 2010, **195**, 3498-3503.
17 V. Neburchilov, H. J. Wang, J. J. Martin and W. Qu, *Journal of Power Sources*, 2010, **195**, 1271-1291.
18 R. N. S. M. Hamdani , P. Chartier, *Int. J. Electrochem. Sci*, 2009, **5**, 556-577.
19 E. Rios, J. L. Gautier, G. Poillerat, P. Chartier, *Electrochimica Acta*, 1998, **44**, 1491-1497.
20 X. Wu and K. Scott, *Journal of Power Sources*, 2012, **206**, 14-19.
21 J. Ponce, J. K. Rehspringer, G. Poillerat, J.L. Gautier, *Electrochimica Acta*, 2001, **46**, 3373-3380.
22 Z. Q. Liu, Q. Z. Xu, J. Y. Wang, N. Li, S. H. Guo, Y. Z. Su, H. J. Wang, J. H. Zhang and S. Chen, *International Journal of Hydrogen Energy*, 2013, **38**, 6657-6662.
23 M. D. Koninck and B. Marsan, *Electrochimica Acta*, 2008, **53**, 7012-7021.
24 C. Jin, F. L. Lu, X. C. Cao, Z. R. Yang and R. Z. Yang, *Journal of Materials Chemistry A*, 2013, **1**, 12170-12177.
25 X. Wang, X. D. Han, M. F. Lim, N. D. Singh, C. L. Gan, M. Jan and P. S. Lee, *The Journal of Physical Chemistry C*, 2012, **116**, 12448-12454.
26 J. W. Xiao, Q. Kuang, S. H. Yang, F. Xiao, S. Wang and L. Guo, *Scientific Reports*, 2013, **3**, 2300-2307.
27 W. W. Liu, C. X. Lu, K. Liang and B. K. Tay, *Journal of Materials Chemistry A*, 2014, DOI: 10.1039/c4ta00107a.
28 C. Z. Yuan, J. Y. Li, L. R. Hou, L. Yang, L. F. Shen and X. G. Zhang, *Journal of Materials Chemistry*, 2012, **22**, 16084-16090.
29 D. U. Lee, B. J. Kim and Z. W. Chen, *Journal of Materials Chemistry A*, 2013, **1**, 4754-4762.
30 I. Nikdov , E. Zhecheva , R. Stoyanova , N. Dimitrow , T. Vitanov *Journal of Electroanalytical Chemistry*, 1997, **429**, 157-168
31 E.B. Castro, C. A. Gervasi, *International Journal of Hydrogen Energy*, 2000, **25**, 1163-1170.
32 J. F. Marco, J. R. Gancedo, M. Gracia, J. L. Gautier, E. I. Ríos, H. M. Palmer, C. Greaves and F. J. Berry, Journal of Materials Chemistry, 2001, 11, 3087-3093.
33 J. Marco, Journal of Solid State Chemistry, 2000, 153, 74-81.
34 J. K. Zhu and Q. M. Gao, Microporous and Mesoporous Materials, 2009, 124, 144-152.
35 T Choudhury, S. Q. Saled, J. L. Sullivan and A. M. Abbot, J. Phys. D: Appl. Phys, 1989, 22, 1185-1195.
36 V.M. Jimenez, A. Fermandez, A. R. Gonzalez-Elipe, *Journal of Electron Spectroscopy and Related Phenomena*, 1995, **71**, 61-71.
37 J. H. Zhong, A. L. Wang, G. R. Li, J. W. Wang, Y. N. Ou and Y. X. Tong, Journal of Materials Chemistry, 2012, 22, 5656-5665.
38 J. H. Kim, D. L. Pugmire, D. Battaglia, M.A. Langell, *Applied Surface Science*, 2000, **165**, 70-84.
39 D. Carriazo, J. Patiño, M. C. Gutiérrez, M. L. Ferrer and F. D. Monte, *RSC Advances*, 2013, **3**, 13690-13695.
40 H. B. Wu, H. Pang and X. W. Lou, *Energy & Environmental Science*, 2013, **6**, 3619-3626.
41 R. Ding, L. Qi and H. Y. Wang, *Journal of Solid State Electrochemistry*, 2012, **16**, 3621-3633.
42 Y. Gou, X. Liang and B. H. Chen, *Journal of Alloys and Compounds*, 2013, **574**, 181-187.
43 Y. Y. Liang, Y. G. Li, H. L. Wang and H. J. Dai, *Journal of the American Chemical Society*, 2013, **135**, 2013-2036.
44 Y. Y. Liang. Y. G. Liang, H. L. Wang, J. G. Zhou, J. Wang, T. Regier and H. J. Dai, *nature materials*, **10**, 780-786.
45 Y. Y. Shao, J. H. Sui, G. P. Yin and Y. Z. Gao, *Applied Catalysis B: Environmental*, 2008, **79**, 89-99.
46 G. V. a. K. J. Stevenson, *Langmuir*, 2007, 23, 5279-5282.
47 Y. Zhang, Y. Hu, S. Li, J. Sun and B. Hou, *Journal of Power Sources*, 2011, **196**, 9284-9289.